Thermal capillary waves in colloid–polymer mixtures in water

2008 J. Phys.: Condens. Matter 20 494231

(http://iopscience.iop.org/0953-8984/20/49/494231)

J. Phys.: Condens. Matter **20** (2008) 494231 (6pp) doi:10.1088/0953-8984/20/49/494231

Thermal capillary waves in colloid–polymer mixtures in water

E A G Jamie, G J Davies, M D Howe, R P A Dullens and D G A L Aarts

Department of Chemistry, Physical and Theoretical Chemistry Laboratory, University of Oxford, South Parks Road, Oxford OX1 3QZ, UK

E-mail: dirk.aarts@chem.ox.ac.uk

Received 31 July 2008, in final form 3 October 2008
Published 12 November 2008
Online at stacks.iop.org/JPhysCM/20/494231

Abstract

We develop two colloid–polymer mixtures in water and study their phase and interface behaviour by means of confocal scanning laser microscopy. The systems consist either of silica or of poly(methylmethacrylate) particles, fluorescently labelled, with, as the polymer, xanthan. The fluid–fluid phase separation can be clearly followed in time and, depending on the concentrations and system details, we observe coarsening either of a bicontinuous spinodal structure or of a suspension of colloid-rich droplets. After phase separation has completed, we study the thermal capillary waves at the fluid–fluid interface. We construct correlation functions and compare with capillary wave theory. Finally, we demonstrate that these colloid–polymer systems are compatible with microfluidics.

1. Introduction

The rapidly evolving field of microfluidics, in which fluids are manipulated at a micro or even nanoscopic scale, raises new questions about the behaviour of liquids at increasingly small scales. One particular topic of interest is the behaviour of interfaces in confinement and under flow, which is for example essential when carrying out chemical reactions in liquid mixtures. At certain lengthscales thermal capillary waves at fluid interfaces may become dominant in the sense that stochastic terms must be included in hydrodynamic descriptions [1–3]. One convenient way to explore these issues is by making use of colloidal systems [4].

We have shown that thermal capillary waves at the interface of a fluid–fluid phase separated colloid–polymer mixture can be directly observed by means of confocal scanning laser microscopy (CSLM) [5]. However, the experimental system was dispersed in an organic solvent (decalin), which is incompatible with microfluidic devices made out of poly(dimethylsiloxane) (PDMS) elastomers, a material frequently used in microfluidics (see e.g. the recent review by Whitesides [6]). To overcome this incompatibility we are left with two options; either change from PDMS to a different material or change the colloid–polymer system such that water, which is compatible with PDMS, is the main dispersing solvent. Several recipes are now available for the first option (see [7, 8] and references therein). Here we will stick to PDMS, because of its beneficial optical and elastic properties, its low cost and the ease of fabrication, and present results deal with the second option.

In order to develop a colloid–polymer mixture in which the thermal interfacial fluctuations can be observed microscopically and in which water is the main dispersing solvent, several conditions have to be met. Firstly, the polymer radius of gyration R_G needs to be at least roughly a third of the colloid radius a in order to give a stable fluid–fluid phase coexistence [9]. The coexistence is between a phase rich in colloids and poor in polymers and one rich in polymers and poor in colloids. The phase separation is microscopically a result of the attractive depletion interaction between the colloids, mediated by the polymers [10, 11]. Secondly, the interfacial tension needs to be of order 10^{-7} N m^{-1}, such that the thermal roughness $L_T = \sqrt{k_B T/\gamma}$ is $\sim$0.2 μm, which is comparable to the in plane resolution of confocal microscopy. Since the interfacial tension γ scales as the thermal energy $k_B T$ over the particle diameter squared [12, 13], the particles need to be $\sim$0.2 μm as well. Thirdly, the colloids and polymers need to be stable in water, the polymer should not adsorb on the colloids and the colloids must be fluorescently labelled. Finally, both polymers and colloids should not stick to PDMS and glass surfaces.

In this paper, we will present results on two experimental systems we have developed. We will start by describing the experimental details in section 2. This will be followed by

the results and a discussion thereof (section 3), where we will look at both bulk and interface behaviour and demonstrate the compatibility of the developed systems with microfluidics. In section 4 we will conclude our main findings.

2. Experimental system

We have developed two different colloid–polymer systems. One consists of silica particles, the other of poly(methylmethacrylate) particles, both fluorescently labelled and dispersed in water. As depletion agent xanthan polymer is used. We will first describe the synthesis methods and properties of the colloidal particles, followed by the properties of the polymer, and finally the mixtures will be discussed.

2.1. Colloidal particles

2.1.1. Silica particles. Here, we followed standard recipes in the literature, mainly [14, 15]. Tetra ethyl orthosilicate (TEOS, 98%) was used as a silica source, with 3-aminopropyltriethoxysilane (APS) as the silane coupling agent. The dye used was rhodamine B isothiocyanate (RITC). Ammonium hydroxide was used as catalyst (25–30% NH_3). The solvent used was ethanol (anhydrous, 200 Proof). All chemicals were sourced from Sigma and used as provided. Excess APS (20 mM) was added to a solution of RITC (5 mM) in 5 ml of ethanol in order to prepare the dye [14]. The mixture was stirred on a magnetic stirring plate for 18 h in the dark to prevent bleaching and to ensure complete coupling of the reagents. Next, two ethanol solutions (25 ml) were prepared. Solution 1 contained ammonium hydroxide (0.4 M NH_3) and deionized water (3.33 M). Solution 2 contained TEOS (0.4 M) and 5 mM of the RITC dye solution, where we have followed relative quantities after Vacassy *et al* [16]. The two solutions were mixed with continuous stirring in the dark for up to 24 h. The resulting product was centrifuged at 1500 rpm to isolate the particles. The supernatant layer was removed, and the product washed in water and re-isolated by centrifugation twice. The dispersing solvent was now predominantly water. Products were characterized by atomic force microscopy (AFM) and scanning electron microscopy (SEM). This particular recipe gave particles with a diameter of 80 nm. By adding sodium dodecyl sulfate as surfactant to ethanol solution 1 the diameter can be increased up to 1.5 μm, see for example [15].

2.1.2. PMMA particles. The poly(methylmethacrylate) particles were prepared using the first part of the emulsion polymerization method by Kumacheva *et al* [17]. All chemicals were sourced from Sigma and used as provided. 0.1 g of potassium persulfate was dissolved in 35 g of water at 80 °C under nitrogen conditions. 1.5 g of methylmethacrylate (MMA) was quickly added to the vigorously stirring mixture and the emulsion was allowed to polymerize for 30 min. These seed colloids were then dyed by adding rhodamine dye dissolved in a small amount of MMA and the reactants were stirred for a further 30 min. The reaction flask was removed from the oil bath and the dispersion was washed thoroughly in water by repeated centrifugation. The particle diameter was found to be 210 nm from scanning electron microscopy pictures. The particle suspension displayed a crystallizing sediment, implying that the size polydispersity is fairly low (much lower than the non-crystallizing silica spheres).

2.2. Xanthan polymer

Xanthan (SKW Biosystems, M_w 4 × 10^6 g mol^{-1}), originally provided by Dr R H Tromp (Nizo, Ede, The Netherlands), was used without purification and the xanthan solution was prepared as described in detail in [18, 19], where exactly the same xanthan batch had been used. The radius of gyration and persistence length are 264 nm and 120 nm, respectively, which implies that the xanthan chains are semi-flexible [18]. The aqueous stock solution at 2 mg ml^{-1} xanthan furthermore contained 0.1 M NaCl and 2 mM NaN_3, the latter to prevent bacterial growth.

2.3. Colloid–polymer mixtures

The particles and polymers were mixed together from stock solutions and homogenized by vigorously shaking the sample by hand. The overall NaCl concentration was ∼25 mM, which means that the Debye length was 2 nm. Due to the optical mismatch between colloids and solvent van der Waals forces were not screened, but the particles were charge stabilized and no signs of irreversible particle aggregation have been observed. The underlying DLVO potential modifies the depletion potential. However, if we compare the depletion potential (for ideal polymers) to the one modified by the DLVO interaction (using typical numbers), we only see significant differences at separations below 15 nm. This is less than 3% of the range of the depletion interaction.

Phase behaviour of silica or PMMA–xanthan mixtures was explored by visual observation of samples, where the formation of an opaque mixture under homogenization by shaking indicated that a phase separation was taking place. The nature of the phase separation was observed by placing the mixture in a cut-off cuvette with a glass microscope slide fixed to the bottom, and imaging the resulting process by confocal microscopy tilted to 90°, similar to the setup described in [20], so that sedimentation could be easily observed. Suitable fluid–fluid separating statepoints were selected for further analysis. The CSLM used was the Zeiss LSM 5 Exciter.

3. Results and discussion

Both the silica and the PMMA systems display proper fluid–fluid demixing phase behaviour at intermediate colloid and polymer concentrations. At too high concentrations the systems gel, whereas at very low concentrations a one phase region is observed. We have seen no signs of polymer adsorption and the polymers seem to be a very efficient depletion agent given the low concentrations needed to induce a phase separation. This is in line with previous observations made in a system with yet another colloidal particle, but with identical polymer [18].

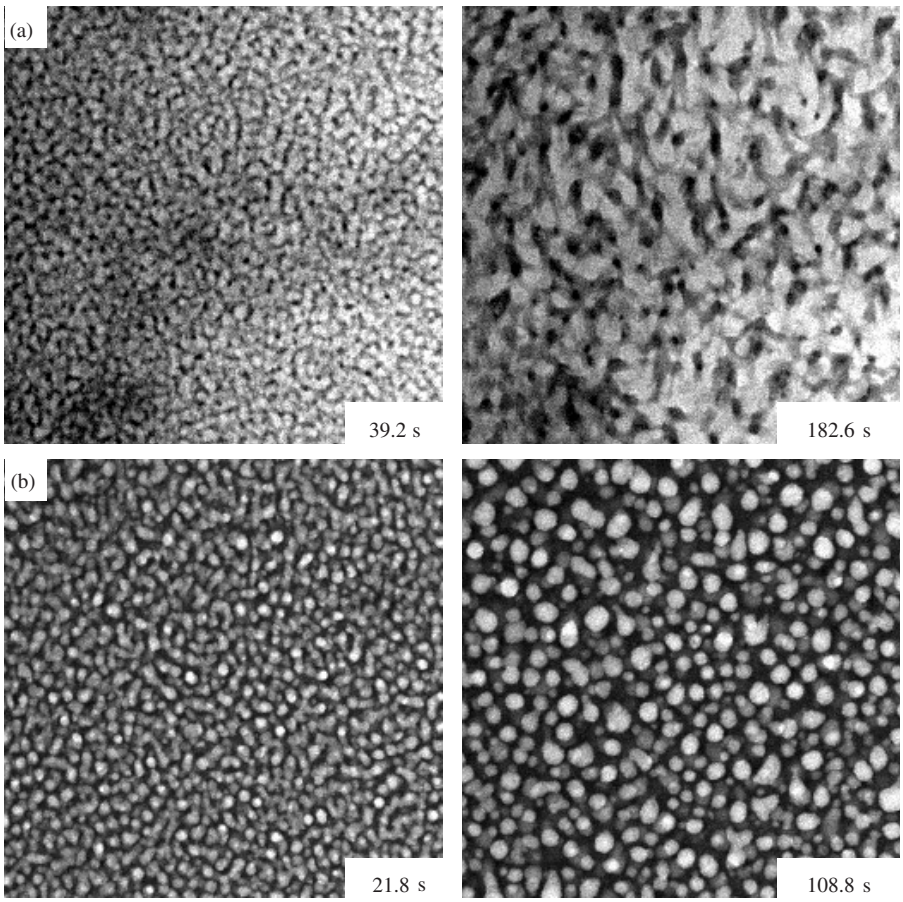

Figure 1. CSLM images showing phase separation in the silica (a) and PMMA (b) systems. Times are with respect to homogenization. The silica system displays a coarsening bicontinuous structure, whereas the PMMA system coarsens through droplet coalescence. Concentrations used are 16 w% silica + 0.046 w% xanthan (a) and 6 w% PMMA + 0.042 w% xanthan (b). The size of the images is 320 × 320 μm^2 and gravity points downwards.

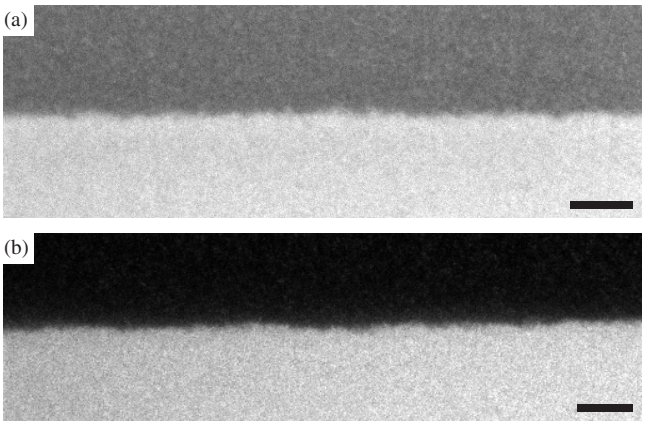

Figure 2. CSLM images of thermal capillary waves in the silica (a) and PMMA (b) system. Concentrations used are 15 w% silica + 0.056 w% xanthan (a) and 32 w% PMMA + 0.046 w% xanthan (b). Scale bars denote 10 μm and gravity points downwards.

Figure 1(a) shows a spinodal decomposition pattern in the silica system, which coarsens in time. Figure 1(b) shows a rather different morphology; at these concentrations the PMMA system exhibits a typical nucleation and growth structure, which coarsens due to coalescence of diffusing droplets of the colloid-rich phase. The different mechanisms stem from different concentrations and polymer to colloid aspect ratios ξ ($\xi = R_G/a$: $\xi_{silica} = 6.6$ and $\xi_{PMMA} = 2.5$), and in both systems nucleation and growth as well as spinodal decomposition have been observed at different statepoints. It is hard to establish if the nucleation and growth mechanism in the PMMA case starts right after homogenization, since the induction time for nucleation and growth might be very short, and the observed droplet structure may also be the result of an initial bicontinuous structure breaking up. Interestingly, however, it becomes clear by inspection of the phase separation movies that the PMMA system in this particular statepoint coarsens through coalescence of diffusing droplets as first posed in [21], and (seemingly) not by Ostwald ripening as described theoretically in [22, 23].

Both structures are affected by gravity when typical lengths become larger than the capillary length and the colloid-rich and polymer-rich phases move in opposite directions. This breaks the symmetry and leads to a macroscopic phase separation as described in great detail in [24].

After typically a couple of hours clean and clear macroscopic interfaces form. Figure 2 shows the interface of the silica (a) and the PMMA system (b). The thermal

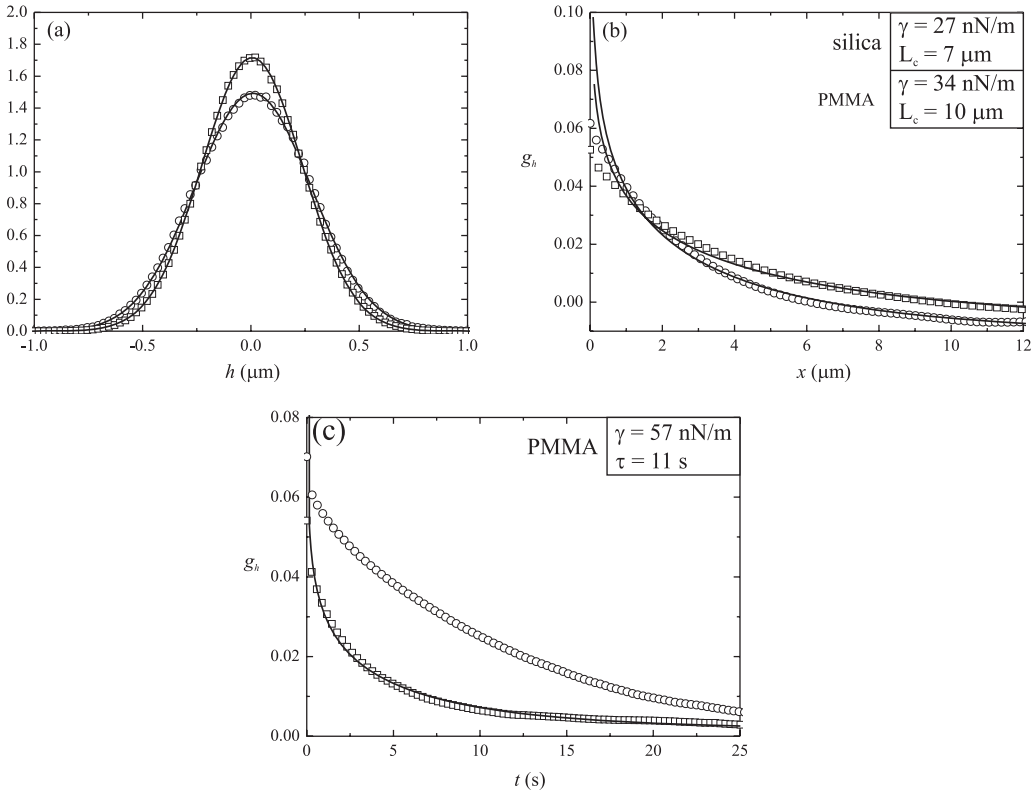

Figure 3. Height distributions (a) and static (b) and dynamic (c) correlation functions in the silica (circles) and PMMA (squares) systems. Same statepoints as indicated in figure 2. Full lines follow from capillary wave theory. The insets show the fitting parameters.

capillary waves at the interface can be easily observed. Similar observations have been made in a range of different systems, but these always consisted of sterically stabilized PMMA particles and polystyrene polymer dispersed in an organic solvent. This is the first time that a system in water and with a biopolymer as depletion agent has been used, which brings the phenomenon and technique much closer to for example the food industry, where polysaccharides such as xanthan are extensively used [25, 26].

To analyse the fluctuations we first locate the interface height in each image by fitting the intensities along each column of pixels with a tangent hyperbolic function [27, 28]. We then may look at a variety of distribution and correlation functions. Figure 3 presents the results. In (a) we have plotted the distribution of heights from the experiment. Both systems display Gaussian height distributions as expected. In (b) and (c) correlation functions are given. In general, we define a correlation function g_h as

$$g_h(x,t) = \langle [h(x',t') - \bar{h}(t')][h(x'+x,t'+t) - \bar{h}(t)] \rangle, \quad (1)$$

where x denotes the coordinate along the interface, t denotes time, and averages are over primed quantities. Furthermore, the height h at any time t is defined with respect to the average height at that time, $\bar{h}(t)$, where the averaging is over space. This is similar to the method followed in [27], but different from the one used in [5]. In the latter case the heights were defined with respect to an average over both space and time. Clearly, a systematic drift in for example the sample position can be dealt with by the first method, although one may lose the longest fluctuations in such case. In general, however, if the total image length along x is much larger than the parallel correlation length, i.e. the capillary length, and if any systematic drifts are small, then the two methods are virtually identical.

Figure 3(b) displays the static correlation function, $g_h(x, t = 0)$. From capillary wave theory originally derived by Mandelstam [29] (for a didactic derivation see for example [30]) we know that each mode with wavevector $\mathbf{q}$ has a mean square amplitude given by

$$\langle |h_{\mathbf{q}}|^2 \rangle = \frac{k_B T}{\gamma L^2} \frac{1}{q^2 + L_c^{-2}}, \quad (2)$$

where the brackets on the left-hand side denote a thermal average, L is the system size, and the capillary length equals $L_c = \sqrt{\gamma/\Delta\rho g}$ with $\Delta\rho$ the mass density difference between the two fluids and g earth's acceleration. This result can be used to fit the data with γ and L_c as physical fitting parameters and an additional constant parameter is used for any baseline offset (a term which is generally small) [5].

The obtained interfacial tensions and capillary lengths have the right order of magnitude compared to previous experiments [5, 28]. However, there is a clear disagreement between the experimental and fitted correlation functions at short lengthscales (below 1 μm). The theoretical prediction no longer accurately describes the data. Here, one expects to find largest deviations from standard capillary wave theory: taking

only the interfacial tension and density difference into account leads to a logarithmically diverging interfacial width, whereas the experimental width remains finite. Therefore, we have taken the somewhat arbitrary choice (see also below) of leaving out the first three data points in the fit, which led to a better overall description. Other possibilities would lie in introducing a q-dependent interfacial tension or similarly adding additional terms to the interface Hamiltonian [31, 32], which we do not explore here. In previous experiments [5] the mismatch at short lengthscales did not announce itself as prominently as in this case. Current observations may have various origins and a possible explanation may be found in the fact that the polymers are much larger than the colloids with a diameter of $2R_G \sim 530$ nm, which is slightly smaller than three pixels, but larger than the in plane confocal resolution. One therefore may speculate about the leading interfacial lengthscale, whether it would originate from the polymer rather than the colloid particle. Furthermore, making the problem more complicated, a third natural lengthscale would be the polymer persistence length, which is comparable to the colloid radius.

The dynamic correlation function, $g_h(x = 0, t)$, is shown in figure 3(c). Theoretically, each mode is exponentially damped by $\exp[-t/2\tau_q]$, with

$$\tau_q = \tau \frac{q L_c}{1 + q^2 L_c^2} \tag{3}$$

where τ is the capillary time, $\tau = \eta L_c/\gamma$, with η the sum of the viscosities of both phases [33, 34]. The density of the phases does not appear, since we are in the overdamped limit (low Reynolds number). Details are given elsewhere on how to fit the real-space data; γ, τ and a baseline correction have been used as fitting parameters [5]. It turns out that only the PMMA data could be fitted using this model. This gives a very accurate description. The interfacial tensions from the dynamic and static correlation functions are in reasonable agreement, especially given the less accurate fit in the static case. Possibly, previously mentioned effects at short lengthscales do not emerge as prominently as in the static correlation function; at short lengthscales the waves are very effectively damped. The reason for not being able to fit the silica data is unknown, but one might wonder for example about visco-elastic effects in xanthan solutions. It is well known that xanthan solutions display shear-thinning effects above certain shear rates, which strongly depends on the overall polymer concentrations (see for details of rheology on this particular xanthan polymer [19]). Although the overall xanthan concentrations are relatively low, it may have considerably increased in the polymer-rich phase and then possibly more so in the silica system than in the PMMA one (please note that due to the very different aspect ratios ξ a direct comparison between the two systems based on the overall polymer concentration is not straightforward). One then wonders if the intrinsic fluctuations of the interface may effectively lead to shear-thinning effects, which could be taken into account by introducing a wavevector dependent viscosity in equation (3) as in the work of Delgado-Buscalioni *et al* [35]. This lies, however, outside the scope of the present work.

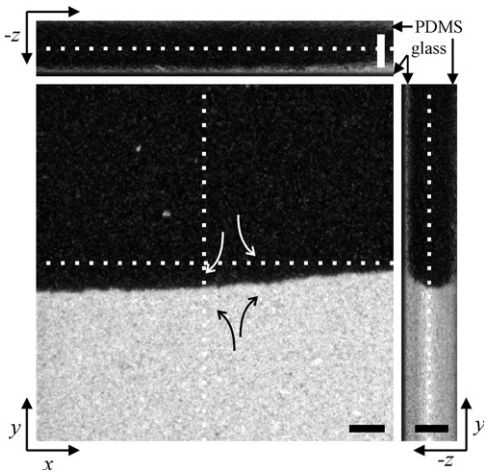

Figure 4. 3D CSLM image of the demixed PMMA system in a microfluidic cell imaged at the stagnation point in a cross-channel. Flow lines are roughly indicated by the arrows. The white dashed lines indicate the positions of the x, y and z images, i.e. the y, z image is taken along the vertical dashed line, for example. The scale bar denotes 10 μm in the long direction. Gravity points along the negative z-axis.

We started by saying that colloid–polymer mixtures are compatible with microfluidics due to the similar lengthscales (e.g. interface roughness, L_c), but that a system in water was needed. Having such a system we show in figure 4 that this may indeed be combined with microfluidics. Presented is a (three dimensional) confocal image of the flow of a colloid-rich and a polymer-rich phase at a stagnation point in a cross-channel. One should particularly note that the fluctuations can be clearly observed, three dimensional information can be easily obtained, and wetting effects are prominent. Both the glass and PDMS walls are wetted by the colloid-rich phase, as is evident from the fluorescent layers in the (x, z) and (y, z) images.

4. Conclusion

We have shown results on two different phase separating colloid–polymer mixtures in water. The confocal microscopy images of the phase separation process demonstrates that we are dealing with fluid–fluid demixing and two different patterns have been distinguished: coarsening of a bicontinuous structure and coarsening due to coalescence in a suspension of diffusing colloid-rich droplets. These observations are worth further exploration. After phase separation has completed, the interface is clearly dynamically rough, which can be analysed in terms of thermal capillary waves. This is in fact the first microscopical observation of this phenomenon in a system with water as the dispersing solvent, underlining the flexibility of the chosen technique and the generality of the phenomenon. From the correlation functions very reasonable interface properties can be obtained, although the capillary wave model should be extended to capture some of the details. Questions arising concern the competing microscopic lengthscales and the rheology of the system. Finally, we have shown the compatibility between the colloid–polymer mixtures

and PDMS based microfluidic devices. This opens up the possibility to study dynamic and static effects in microfluidics at unprecedented detail.

Acknowledgment

It is a pleasure to thank Didi Derks for useful discussions.

References

[1] Moseler M and Landman U 2000 *Science* **289** 1165
[2] Eggers J 2002 *Phys. Rev. Lett.* **89** 084502
[3] Davidovitch B, Moro E and Stone H A 2005 *Phys. Rev. Lett.* **95** 244505
[4] Hennequin Y, Aarts D G A L, van der Wiel J H, Wegdam G, Eggers J, Lekkerkerker H N W and Bonn D 2006 *Phys. Rev. Lett.* **97** 244502
[5] Aarts D G A L, Schmidt M and Lekkerkerker H N W 2004 *Science* **304** 847
[6] Whitesides G M 2006 *Nature* **442** 368
[7] Bartolo D, Degré G, Nghe P and Studer V 2007 *Lab Chip* **8** 274
[8] Abate A R, Lee D, Do T, Holtze C and Weitz D A 2008 *Lab Chip* **8** 516
[9] Lekkerkerker H N W, Poon W C K, Pusey P N, Stroobants A and Warren P B 1992 *Europhys. Lett.* **20** 559
[10] Asakura S and Oosawa F 1954 *J. Chem. Phys.* **22** 1255
[11] Vrij A 1976 *Pure Appl. Chem.* **48** 471
[12] De Gennes P G 1979 *Scaling Concepts in Polymer Physics* (Ithaca: Cornell University Press)
[13] Widom B 1975 Critical phenomena *Fundamental Problems in Statistical Mechanics* vol 3, ed E G D Cohen (New York: Elsevier)
[14] van Blaaderen A and Vrij A 1992 *Langmuir* **8** 2921
[15] Lee M H, Beyer F L and Furst E M 2005 *J. Colloid Interface Sci.* **288** 114
[16] Vacassy R, Flatt R J, Hofmann H, Choi K S and Singh R K 2000 *J. Colloid Interface Sci.* **227** 302
[17] Kumacheva E, Kalinina O and Lilge L 1999 *Adv. Mater.* **11** 231
[18] Koenderink G H, Aarts D G A L, de Villeneuve V W A, Philipse A P, Tuinier R and Lekkerkerker H N W 2003 *Biomacromolecules* **4** 129
[19] Koenderink G H, Sacanna S, Aarts D G A L and Philipse A P 2004 *Phys. Rev.* E **69** 021804
[20] Aarts D G A L and Lekkerkerker H N W 2004 *J. Phys.: Condens. Matter* **16** S4231
[21] Binder K and Stauffer D 1974 *Phys. Rev. Lett.* **33** 1006
[22] Lifshitz I M and Slyozov V V 1961 *J. Phys. Chem. Solids* **19** 35
[23] Wagner C 1961 *Z. Electrochem.* **65** 581
[24] Aarts D G A L, Dullens R P A and Lekkerkerker H N W 2005 *New J. Phys.* **7** 40
[25] Parker A, Gunning P A, Ng K and Robins M M 1995 *Food Hydrocolloids* **9** 333
[26] Katzbauer B 1998 *Polym. Degrad. Stab.* **59** 81
[27] Derks D, Aarts D G A L, Bonn D, Lekkerkerker H N W and Imhof A 2006 *Phys. Rev. Lett.* **97** 038301
[28] de Villeneuve V W A, van Leeuwen J M J, de Folter J W J, Aarts D G A L, van Saarloos W and Lekkerkerker H N W 2008 *Europhys. Lett.* **81** 60004
[29] Mandelstam L 1913 *Ann. Phys.* **41** 609–24
[30] Vrij A 1966 *Discuss. Faraday Soc.* **42** 23
[31] Mecke K R and Dietrich S 1999 *Phys. Rev.* E **59** 6766
[32] Hiester T, Dietrich S and Mecke K 2006 *J. Chem. Phys.* **125** 184701
[33] Jeng U S, Esibov L, Crow L and Steyerl A 1998 *J. Phys.: Condens. Matter* **10** 4955
[34] Meunier J 1988 Experimental studies of liquids at interfaces: classical methods for studies of surface tension, surface wave propagation and surface thermal modes for studies of viscoelasticity and bending elasticity *Liquids and Interfaces* ed J Charvolin, J F Joanny and J Zinn-Justin (New York: North-Holland) pp 327–69
[35] Delgado-Buscalioni R, Chacón E and Tarazona P 2008 *J. Phys.: Condens. Matter* **20** 494229